



Towards a better consideration of the interface bonding conditions in the design of bonded concrete overlays

Kristina Bayraktarova · Lukas Eberhardsteiner  · Martin Johannes Peyer · Martin Peyerl · Ronald Blab

Received: 26 August 2022 / Accepted: 6 January 2023 / Published online: 7 February 2023
© The Author(s) 2023

Abstract This study investigates the effect of the interface bonding conditions between a concrete overlay and the existing hot mix asphalt layer on the design life of bonded concrete overlays. Most of the current design approaches assume a full bonding between the layers and ignore the proposed models in the literature for the description of the interlayer behaviour. A reason for that is that these models are very extensive and require big computation effort. To overcome this limitation, this paper analyses temperature-dependent experimental data, that describes the bond behaviour in normal and tangential direction and involves this data in different 3D finite element (FE) models for the evaluation of the impact of the interface bonding conditions on the pavement response.

Further, the effect of applying different interface modelling approaches (full bonding model, friction model and the cohesive zone model (CZM)) in a commercial FE-software on the resulting design life has been demonstrated. One of the most significant findings to emerge from this study is that the implementation of temperature-dependent empirical data to describe the interface bonding conditions leads to more realistic design results.

Keywords Interface bonding · Pavement design · White topping · Bonded concrete overlays

K. Bayraktarova (✉) · L. Eberhardsteiner (✉) ·
M. J. Peyer · R. Blab
Institute of Transportation, Vienna University of
Technology, Karlsplatz 13/E230-03, 1040 Vienna, Austria
e-mail: kristina.bayraktarova@tuwien.ac.at

L. Eberhardsteiner
e-mail: lukas.eberhardsteiner@tuwien.ac.at

M. J. Peyer
e-mail: martin.peyer@tuwien.ac.at

R. Blab
e-mail: ronald.blab@tuwien.ac.at

M. Peyerl
ALAS Minerals GmbH, Unterthalamstraße 2,
4694 Ohlsdorf, Austria
e-mail: m.peyerl@alas.at

1 Introduction

A good bond between the concrete overlay and the hot mix asphalt layer (HMA) ensures the transfer of stresses across the interface and thus the durability of the pavement structure. The bond is normally generated by the interlocking action of the aggregates and the adhesion due to the chemical bond of the cement paste [1]. The interlocking action of the aggregates is provided by the substrate surface preparation (roughness) [1]. Surface preparation includes milling of existing asphalt to eliminate or reduce surface distortions and to help provide a good bond, and surface cleaning.

Considerable experimental research has been conducted regarding the evaluation of pavement interface



bonding and its effect on the pavement performance. Most of these studies investigate the interface between asphalt layers [2–7]. Some of them focus on the interface bonding between concrete slabs and an asphalt overlay [8–11] and only a few of them on the concrete-asphalt interface in bonded concrete overlays of asphalt pavements [12, 13].

Further, when discussing the effect of interface bonding on the pavement performance, it is important to make reference to the several design procedures for concrete overlays that have been developed over the years [14–19]. Each procedure incorporates different inputs, software and has specific design assumptions, deficiencies and strengths [20, 21]. Unfortunately, there is yet no design procedure that considers the real interface bond characteristics between the asphalt and the concrete overlay. Most pavement design methods consider fully bonded layers [14, 16, 18], despite the fact that excessive normal tensile stresses and horizontal shear stresses can lead to debonding and failure [22]. ACPA [23] recognizes that the two most common reasons for failure of the bonded concrete overlay on asphalt are delamination stemming from failure in the bond plane or from failure in the underlying asphalt layer. This method evaluates bond plane stresses using horizontal shear data. It calculates stresses and strains for each mode and compares those against probabilistic models of each mode to determine which factor is the most likely mode of failure, or the weakest link, driving failure in the overall system [23]. Further, a performance based design method for concrete overlays was proposed in [24–26], which considers the residual bearing capacity of the existing HMA-layer, its thickness and temperature-dependent interface bonding characteristics between the existing HMA and the new concrete layer.

In addition, various models have been used to investigate the interlayer behaviour of pavement structures [9, 27–31]. The linear elastic fracture mechanics (LEFM) approach assumes that the interface is having some well-known intrinsic defects and, hence, is not capable of predicting damage between two layers [31]. For this reason, the majority of recent studies uses the powerful computationally efficient Cohesive Zone Model (CZM) that can be applied to predict cracking in homogeneous and non-homogeneous materials and represents non-linear softening behaviour occurring along the fracture process zone in terms of traction separation behaviour. Barenblatt [32]

proposed the CZM to investigate perfectly brittle materials, while Dugdale [33] adopted a fracture process zone concept to study ductile materials exhibiting plasticity. Xu and Needleman [34] presented a potential-based model, where cohesive elements were inserted along either lines or regions in advance by means of the finite element method following an exponential cohesive law. Camacho and Ortiz [35] proposed a similar cohesive law. As the model by Xu and Needleman induces artificial compliance due to the elasticity of the intrinsic cohesive law, Geubelle and Baylor [36] and Espinosa and Zavattieri [37] proposed a bilinear model to alleviate the artificial compliance due to the initial pre-peak slope of the intrinsic cohesive model. Some researchers [28, 31, 38, 39] applied successfully the CZM to address fracture in viscoelastic materials. Olubanwo [29, 40] used an approach based on plane strain analysis within the context of Interface Cohesive Zone Model (ICZM) as viable for describing and predicting delamination mode of failure in bonded concrete overlays systems (BCOs). The study demonstrates the significance of numerical computational tools in resolving the complexity associated with interfacial delamination problems. Cohesive elements and CZM are also implemented into some FE commercial softwares that allow for the effective analysis of fracture initiation and propagation in pavement models.

Having all this in mind, it can be concluded that a more advanced estimation of relevant stresses and strains in the pavement structure would consider in greater detail the effect of the interface conditions between the layers. Such considerations could expand the capability of design methods and better predict the pavement performance. Therefore, this paper discusses the importance of considering the interface bonding conditions between the concrete overlay and the existing HMA layer in the design procedure. Hence, the CZM implemented in the software Abaqus is proposed to characterise the interface bonding conditions which are represented by the consideration of empirical data in the model. Additionally, the impact of using different modelling approaches on the estimation of relevant stresses and on the resulting design life has been investigated.



2 Modelling of the interface bonding conditions

Modelling a pavement structure with different loadings, interactions between the layers and boundary conditions requires a more sophisticated method than the analytical methods. A correlation between different material parameters, slab dimensions, loadings and interactions, and the resulting stresses and strains can be effectively established by the use of finite element models. Hence, different FE-models have been created with the software Abaqus [41]. An important feature of this software is the implementation of different interaction models. This section focuses on the characterisation of the bonding conditions between the concrete and asphalt layers.

For the purpose of this study the CZM was applied to characterise the interface behaviour between the concrete and asphalt layers. A surface based cohesive behaviour implemented in Abaqus was used in the modelling as a interaction property. It provides a simplified way to model cohesive connections with negligibly small interface thicknesses using the traction-separation constitutive model. As Fig. 1 shows, normal τ_n and shear stresses τ_s, τ_t are related to the normal δ_n and shear δ_s, δ_t separations across the interface before the initiation of damage. At $\tau_n^{max} (\tau_s^{max}, \tau_t^{max})$ the cohesive strength is reached, the damage initiates with first micro cracks and the separation begins. After that the damage grows with the increase of the separation until the traction becomes zero. At $\delta_n^f (\delta_s^f, \delta_t^f)$ the layers are completely separated and the interface fails (damage evolution). The fracture energy, G_c , is calculated as the area under the

traction-separation curve and represents the dissipated energy dissipated for crack formation. The stiffness matrix is formed from the shear stiffness components K_s and K_t and the normal stiffness component K_n [41].

The characteristic parameters describing the bilinear traction-separation law between concrete and asphalt in normal and tangential direction can be obtained from pull-off resistance tests according to ÖNORM B 3639-2 [42] or wedge splitting tests according to RVS 13.01.51 [43] and shear resistance tests according to ÖNORM B 3639-1 [44]. In Austria, the shear resistance test and the pull-off tensile resistance test are standardly used for the investigation of the layer bonding in asphalt pavements, where specimens are loaded in shear and normal directions, respectively. The wedge-splitting test is used to test the notch-gap tensile strength and the specific fracture energy in concrete pavements. A detailed description of the tests setups is given elsewhere [42, 44, 45].

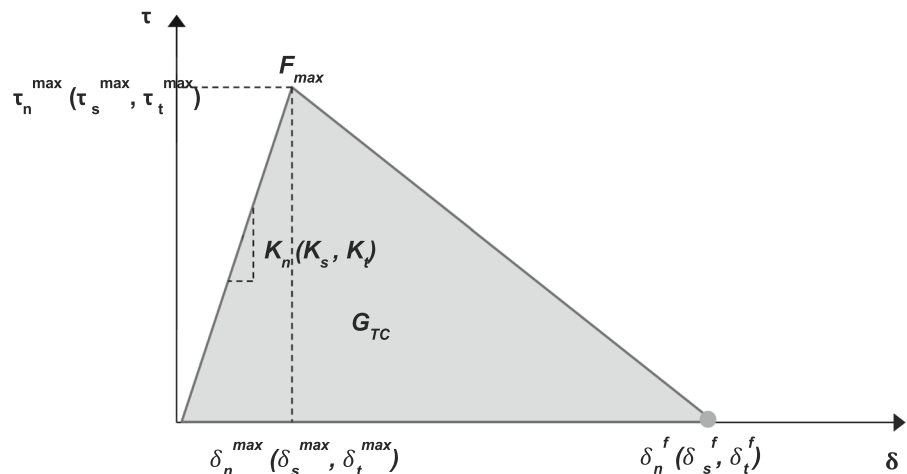
The shear strengths τ_s and τ_t , respectively, (maximum tangential cohesive traction) in $[N \cdot mm^{-2}]$ can be calculated by using the following equation

$$\tau_s = \tau_t = \frac{F_{s,max}}{A} \tag{1}$$

where $F_{s,max}$ is the measured maximum shear force in N and A is the area of the cross section of the specimen in $[mm^2]$.

According to [41] and [46] the tangential cohesive stiffness $K_s=K_t$ can be obtained from the shear strength τ_s and the displacement δ_s^{max} measured when $F_{s,max}$ is reached

Fig. 1 Constitute law for fracture behaviour



$$K_s = K_t = \frac{\tau_s}{\delta_s^{max}}. \quad (2)$$

As mentioned above the normal cohesive traction can be τ_n obtained from a pull-off tensile resistance test or from a wedge splitting test. The pull-off resistance is determined by the maximum reached tensile force $F_{n,max}$ in correlation to the area of the specimen cross section A :

$$\tau_n = \frac{F_{n,max}}{A}. \quad (3)$$

From the determined pull-off strength τ_n and the displacement δ_n^{max} measured when $F_{n,max}$ is reached, the adhesive tensile stiffness K_n can subsequently be derived according to equation

$$K_n = \frac{\tau_n}{\delta_n^{max}}. \quad (4)$$

The wedge splitting test is a displacement controlled test and is performed with a loading velocity of $0.5 [mm \cdot min^{-1}]$ in the vertical direction. After the test, a load–displacement curve can be gained automatically and the fracture mechanical parameters can be determined from test results. The specific fracture energy G_{TC} can be calculated by integration

$$G_{TC} = \frac{1}{A} \int_0^\delta F_{n,max} d\delta_n^{max}, \quad (5)$$

where δ_n^{max} is the horizontal displacement, A is the projected area, $F_{n,max}$ is the maximum horizontal force, and δ is the maximum horizontal displacement of the cutting banks. The nominal notch tensile strength τ_n can be calculated from the maximum horizontal load $F_{n,max}$ using

$$\tau_n = \frac{F_{n,max}}{bh(1 + \frac{6y}{h})}, \quad (6)$$

where h and b are the height and the width of the fracture surface area, respectively, and y is the vertical distance of the centre of gravity of fracture surface from the horizontal force. The nominal notch tensile strength comprises the contribution of tensile stress and flexural stress.

In a subsequent step the shear resistance test according to the Austrian standard ÖNORM B 3639-1 [44] has been modelled in order to investigate the compatibility of experimental results from the

bonding test with the surface-based cohesive model in Abaqus.

The model in Fig. 2 consists of a 40 [mm] thick concrete layer on top of a 40 [mm] thick HMA layer. Both assemblies have a diameter of 100 [mm]. The material properties of the layers at 20 °C are given in Table 1. Both parts are meshed with solid brick elements with a size of 5 [mm] with a total number of elements 18476 each. While the HMA layer is fixed in each direction, the concrete layer is fixed only in x - and y -direction so that it can move in direction z . In the z -direction a measured displacement from the static shear resistance test is applied. The interface bond conditions are simulated with the cohesive zone model as an interaction property, where experimental data from shear resistance and pull-off resistance tests on cores from a road section with white topping was utilized (Table 2). The damage evolution $\delta_n^f(\delta_s^f)$ is the only parameter that has been appraised iteratively.

Figure 3 shows a comparison of the force-displacement curves from the shear resistance test and from the simulation. The considered CZM here is linear and the increasing branch of the curve can therefore only be approximated linearly. However, in the crucial points (points of failure, decreasing branch) the model fits very well. It can be concluded that the actual interface bonding behaviour of the tested specimen was reliably modelled. Therefore, the application of the CZM as an interaction property between layers appears to be

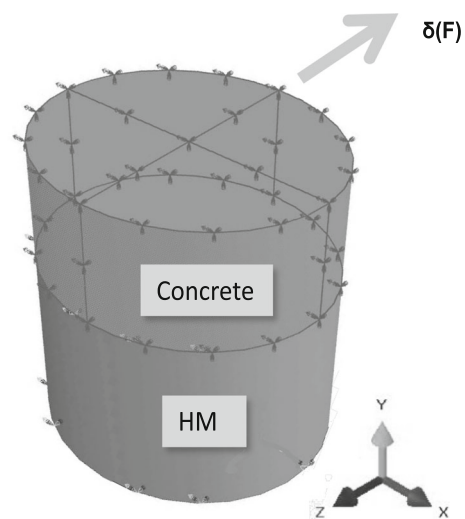


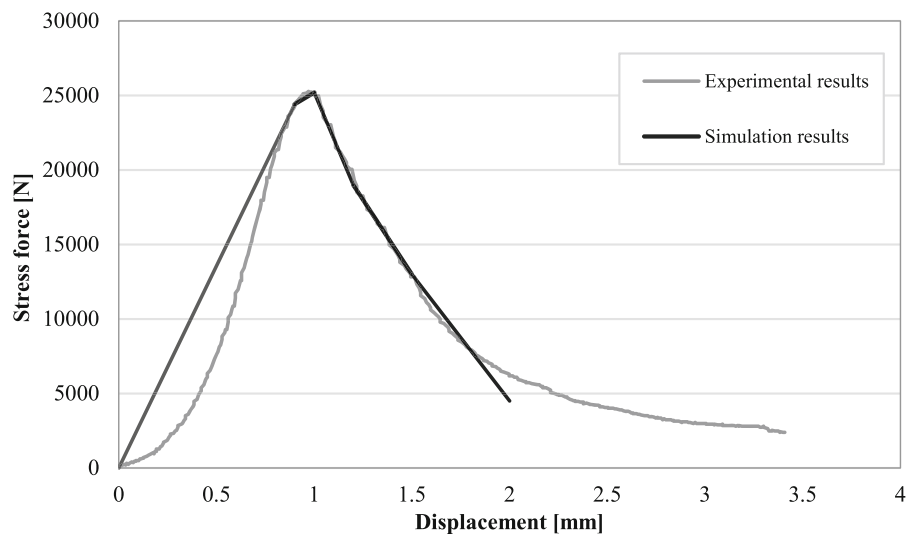
Fig. 2 Simulation of the static shear resistance test

Table 1 Material properties

Layer	E-Modulus at 20 °C [$N \cdot mm^{-2}$]	ν	Density [$kg \cdot mm^{-3}$]
Concrete	30000	0.15	$2.40 \cdot 10^{-5}$
HMA	3500	0.4	$2.20 \cdot 10^{-5}$

Table 2 Interface bond properties

Temperature [°C]	Normal stress τ_n^{max} [$N \cdot mm^{-2}$]	Shear stress $\tau_s^{max} = \tau_t^{max}$ [$N \cdot mm^{-2}$]	Normal stiffness K_n^{max} [$N \cdot mm^{-3}$]	Shear stiffness $K_s^{max} = K_t^{max}$ [$N \cdot mm^{-3}$]	Damage evolution $\delta_s^f = \delta_t^f$ [mm]
20	2.89	3.22	1.84	3.31	2.49

Fig. 3 Comparison of the force-displacement curves from the shear resistance test and from the simulation

feasible for the estimation of critical stresses and strains in pavement structural models.

3 Experimental investigation of the temperature-dependent bond characteristics

The main goal here is the assessment of the bonding parameters between the concrete overlay and the HMA layer. As the behaviour of the HMA layer is strongly temperature-dependent, this should be considered in the modelling of the interface and in the design of bonded concrete overlays. For this reason, cores were taken from two test tracks and examined at different temperatures using the three above mentioned bonding test methods.

3.1 Test sections and sampling

The first test track was built in 2014 as part of the project “Urban Traffic Surface – Optimized concrete for inner-city areas” [47]. The rigid pavement (with a thickness of 12 [cm]) was constructed according to the usual methods for white topping. The surface of the asphalt layer was milled in longitudinal direction before layering the concrete. No tack coat was used. The test track has been used as a parking area for construction equipment and has not been exposed to real traffic. Five years after the construction cores were extracted and tested using the above described test methods.

The second test track was built in 2018 on the regional road L45 between Stratzdorf and Rohrendorf (km 4.050–4.200). In this project, the HMA top layer

was conventionally milled in the driving direction and replaced with a 10 or 12 [cm] thick concrete layer. The test section was divided into individual fields with different layer thicknesses and joint spacings. The used concrete mixture has a maximum aggregate size of 22 [mm]. No tack coat was applied before layering the concrete. Close to the test section there is an operational gravel pit and therefore a significant amount of heavy traffic has been expected to pass the section daily. Cores were extracted from this road section in 2021 to examine the interface bonding properties between the concrete and the asphalt layer.

Table 3 gives an overview of the testing program and the number of extracted cores from both test sections. As the samples from the second section were taken two years after the examination of the first one, the knowledge gained from the first examination was considered when determining the test program for the second section. The pull-off and wedge splitting tests on samples from the first test track at 40 °C were not evaluated because the failure during the testing occurred in the asphalt layer and not at the interface between the two layers. For this reason a maximum test temperature of 30 °C was defined for the specimens obtained from the second test track.

3.2 Results

This chapter analyses the results from the laboratory tests and discusses the implementation of the obtained experimental results in the design of white topping pavement structures.

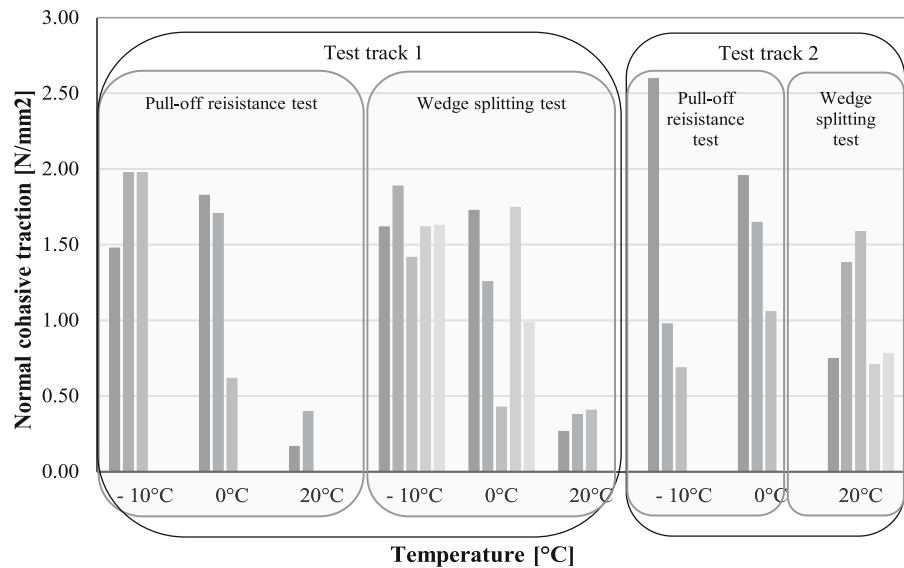
3.2.1 Normal cohesive behaviour

Pull-off resistance tests and wedge splitting tests are employed to identify parameters, which can be used in the CZM to characterise the interface behaviour in normal direction. Hence, tests are carried out at four test temperatures (−10 °C, 0 °C, 20 °C and 30 °C or 40 °C).

However, the pull-off resistance tests and the wedge splitting tests on cores from the first test section failed at 40 °C. Therefore, it was decided to try to conduct them at 30 °C for the second test track. At 30 °C the failure occurred again in the asphalt and not at the interface. This indicates that at high test temperatures the tensile strength of the asphalt is lower than the tensile strength of the interface. The results of three specimens from the first test track at 20 °C were also not evaluated because cracks occurred in the HMA during the tests.

Table 3 Testing program and sampling

Laboratory tests	Testing temperature °C	Extracted cores	
		Test track 1	Test track 2
Shear resistance test	−10	3	3
	0	3	3
	20	3	3
	30	-	3
	40	3	-
Pull-off resistance test	−10	3	3
	0	3	3
	20	3	-
	30	-	3
	40	3	-
Wedge splitting test	−10	5	-
	0	5	-
	20	5	5
	30	-	-
	40	5	-

Fig. 4 Normal cohesive traction

The results from the preliminary experimental work on cores from both test tracks are summarised in Fig. 4. The normal cohesive traction is represented by the adhesive tensile strength and by the notch tensile strength. It is apparent from this figure that the temperature is a factor, which influences the interface behaviour significantly. Despite the wide dispersion of the results, it is obvious that the tensile strength decreases with the increase of temperature. There are several possible reasons for the scatter between individual test results at each temperature. The most probable one is an inhomogeneous condition of the old HMA layer. As mentioned above, the tested cores were extracted from road sections, which were rehabilitated with a BCO. The old HMA layer was milled prior to the BCO placement in order to remove the rutting, restore the levelling and ensure the composite action between the concrete overlay and the old HMA layer. However, this procedure, together with the repair of any further visual defects can not fully ensure that the HMA is in a good and homogeneous condition. Another reason for this scatter could be that some samples were pre-damaged without any visual defects during the drilling, extraction and transport. Further defects could have occurred during the construction process, e.g. construction at low temperatures, bad compaction etc. This was considered when choosing the test data for the derivation of the CZM parameters.

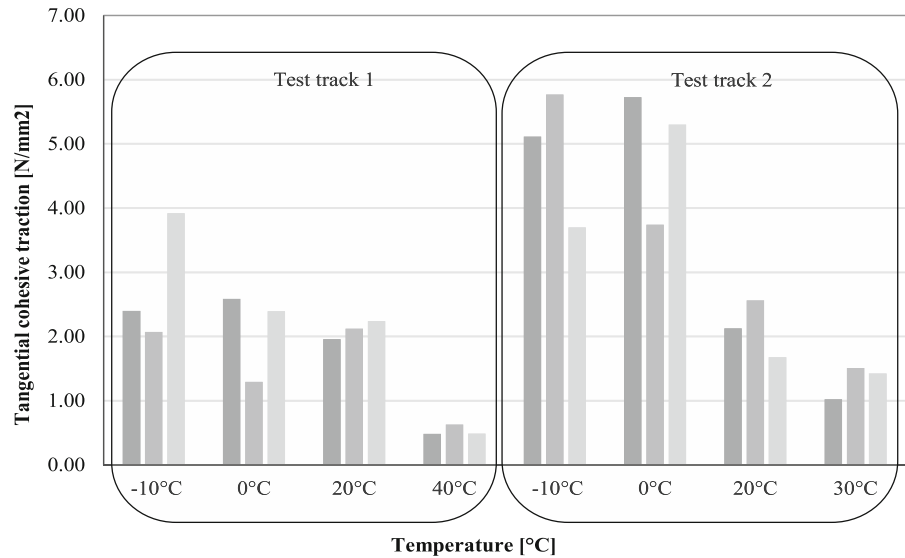
When comparing the tensile strengths obtained from the pull-off resistance and from the wedge splitting tests on cores from the first test track, it can be seen that they are in same range of values. Due to the large scatter of the results from both test tracks it is difficult to assess where the strengths are higher. However, the tensile strength at 20 °C at the second test track is almost twice as higher as at the first one.

3.2.2 Tangential cohesive behaviour

Shear resistance tests were performed to derive parameters describing the interface behaviour in tangential direction. Figure 5 provides the results obtained from testing cores from both test tracks. Three specimens were tested at each temperature (−10 °C, 0 °C, 20 °C and 30 °C or 40 °C). In contrast to the tensile tests, the conduction of shear resistance tests was successful at all examination temperatures. However, to correlate with the examination program for the tensile tests, the maximum testing temperature for shear tests at the second test track was set also at 30 °C.

Figure 5 reveals that the resulting shear strengths at low temperatures from the second test track are much higher than those from the first one. This can be explained by the fact that the traffic at the second section was released 3 days after the concrete placement, which caused an additional compaction of the concrete and thus better aggregate interlocking. At the same time, there was no real traffic on the first test

Fig. 5 Tangential cohesive traction



section during the whole exploitation time. The scatter of the results at higher test temperatures is smaller than at low temperatures.

Similar to the tensile strength tests, the shear strength decreases with rising test temperature. This indicates again the profound effect of the temperature on the interface bond behaviour. From Fig. 5 it is noticeable that the values of the shear strength at -10°C and 0°C are in the same range. Further, the results from the second test section at -10°C and 0°C are almost identical. A possible explanation for this might be that at low temperatures the adherent effect of the bitumen is not activated. In this case, transfer of the shear force is ensured by the aggregate interlocking (friction), which is not temperature-dependent.

4 Impact of the bonding conditions on the design service life

4.1 Investigation the occurring stresses due to traffic loading

To demonstrate the impact of different bonding conditions and modelling approaches on the occurring stresses and later, respectively, on the design life of bonded concrete overlays, two FE models of pavement structures with different geometries were created with the software Abaqus (Fig. 6). Figure 6 shows the finite element mesh and the approximate size of the used

quadratic bricks (C3D8, C3D8R and C3D20R according to ABAQUS' nomenclature). These models consist of four layers, whose material properties are given in Table 4. The moduli of the HMA, base and subgrade layers have been varied depending on the season period (P1, P2, P3 and P4). In order to investigate realistic cases from the practice, a residual bearing capacity of the HMA layer from 70 % of the initial bearing capacity has been considered. Together with the different interface modelling approaches the concrete overlay thickness was also varied (120 mm, 160 mm and 200 mm).

Along the longitudinal edge of the pavement, a shoulder was modelled as an unbound layer in order to reproduce the real boundary conditions. The interaction between the shoulder and the slabs has been represented by a penalty friction model with a friction coefficient of 0.1. Furthermore, a symmetry axis was applied along the other edge of the pavement. The aggregate interlocking in the undoweled joints is simulated also by a penalty friction formulation with a friction coefficient of 0.9. Additionally, a penalty frictional interface with $\mu = 0,5$ was applied between the HMA and the base layer. The bottom of the subgrade is fixed in each direction and a surface-based tie constraint is modelled between the base layer and the subgrade.

The interface modelling approach between the concrete and the HMA-layer has been varied with (i) a full bonding model, (ii) a penalty friction model and

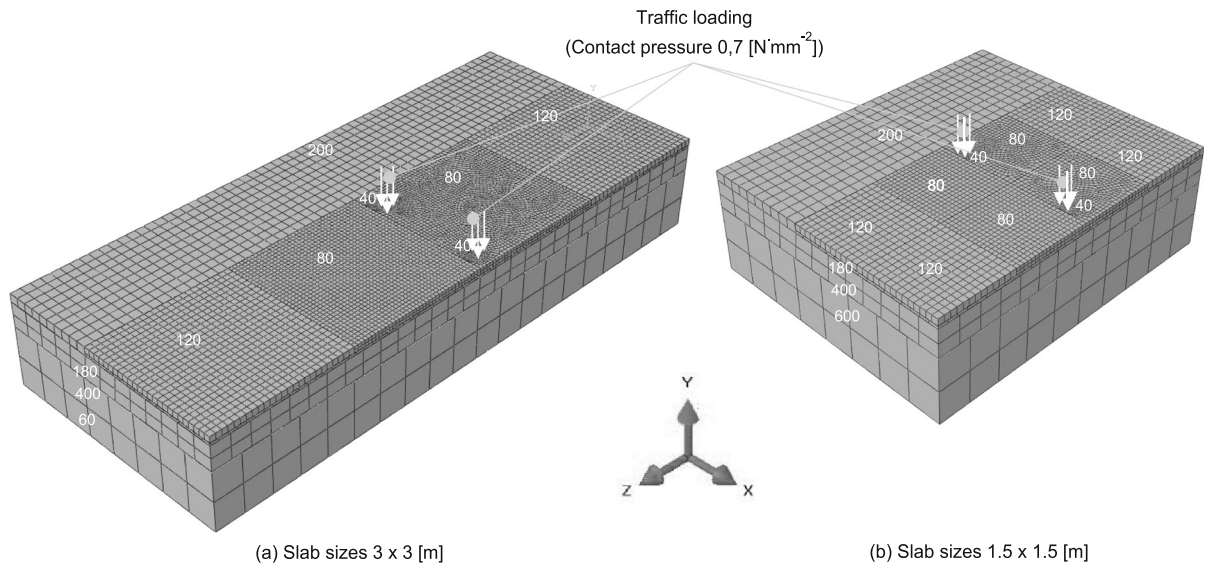


Fig. 6 FE mesh models

Table 4 Material properties

Layer	E-Modulus [$N \cdot mm^{-2}$]				ν	Density [$kg \cdot mm^{-3}$]	Thickness [mm]
Concrete	30000				0.15	$2.40 \cdot 10^{-5}$	120, 160 and 200
Asphalt ^a	12244	1959	551	12244	0.40	$2.20 \cdot 10^{-5}$	50
Base layer	678	169	242	339	0.35	$1.80 \cdot 10^{-9}$	500
Subgrade	280	70	100	140	0.35	$1.80 \cdot 10^{-9}$	1200

^aResidual Bearing Capacity of the asphalt layer of 70%

(iii) a cohesive zone model. In the cases where the full bonding and the friction model were applied, the material parameters were taken from Table 4.

The input parameters for CZM rely on the experimental results from Chapter 3.2 from the second test track at 0 °C, 20 °C and 30 °C. The mean value of the shear strength and, respectively, of the pull-off resistance at each test temperature were determined and then test results with values close to the mean were defined as representative (see Table 5). The considered temperatures were assigned in a subsequent step to the four seasonal periods with varying subgrade moduli.

Thus, four additional cases with the utilisation of the CZM were defined for the parameter study in Table 6. The material properties of the concrete, base and subgrade layers are taken from Table 4.

The traffic load is represented by a single axle load of 100 [kN], which is modelled as uniform pressure over a circular area with radius of 150.79 [mm] with a contact pressure of 0.7 [$N \cdot mm^{-2}$]. The distance between these two circular areas is 2.50 [m], which is typical for HGVs. Furthermore, the position of the load is different at each joint pattern and depends on the width of the sealed carriage way. The axle is always placed in the middle of the lane and the considered maximum stresses are under the wheels (at the bottom of the concrete layer).

Figure 7 shows the resulting maximum stresses due to traffic from the different interface modelling approaches and slab geometries for seasonal period 4. When comparing Fig. 7a with Fig. 7b and, respectively, Fig. 7c with Fig. 7d, it is obvious that the joint spacing has almost no effect on the stresses due to

Table 5 Temperature-dependent interface bond properties for the CZM

Temperature [°C]	Period P	Normal stress t_n^{max} [N · mm ⁻²]	Shear stress $\tau_s^{max} = t_t^{max}$ [N · mm ⁻²]	Normal stiffness K_n^{max} [N · mm ⁻³]	Shear stiffness $K_s^{max} = K_t^{max}$ [N · mm ⁻³]	Damage evolution $\delta_s^f = \delta_t^f$ [mm]
0	P1 ^a	1.65	3.74	1.33	2.54	1.60
20	P2 ^b	0.70	2.13	1.30	1.25	5.00
30	P3 ^c	0.40	1.43	0.44	0.61	4.20
0	P4 ^d	1.65	3.74	1.33	2.54	1.60

^a Winter (December 16 to March 15)

^b Spring (thawing) (March 16 to May 15)

^c Pre-summer (May 16 to June 15)

^d Summer/fall (June 16 to December 15)

Table 6 Cases with the utilisation of the CZM

Case	Interface bond properties	HMA stiffness [N · mm ⁻²]
CZM (0 °C)	Constant for all periods at 0 °C (Table 5)	12244
CZM (20 °C)	Constant for all periods at 20 °C (Table 5)	1959
CZM (30 °C)	Constant for all periods at 20 °C (Table 5)	551
CZM period dependent	Period dependent (Table 5)	

traffic, whereas an increase of the slab thickness leads to a significant stress reduction. The impact of the different interface modelling approaches on the resulting stresses increases with the decrease of the slab thickness.

The full bonding modelling approach yields the lowest stresses due to traffic, while the highest stresses result from the friction model with a friction coefficient of 0.1. However, it should be noted that the stress in x-direction σ_x (Fig. 6) is in all cases higher than the stress in z-direction σ_z except in the case where the full bonding approach was applied. Higher σ_z in the longitudinal direction indicates that the model can not sufficiently differentiate between the single slabs and estimates the stresses as if the concrete layer is constructed without transverse joints. This is a very interesting finding because it suggests that the full bonding approach can not adequately simulate the structural behaviour of the concrete overlay. However, to ensure the comparability of the results from the further estimations, the stresses in x-direction σ_x were analysed for all cases.

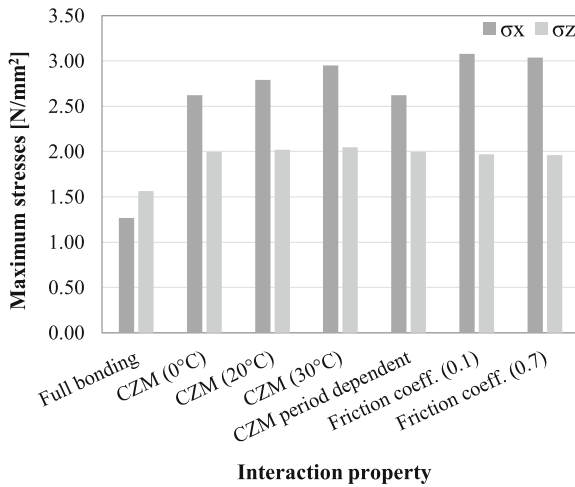
Figure 7 indicates also that the occurring maximum stresses due to traffic are also temperature-dependent.

The maximum stresses due to traffic occur at 30 °C for CZM. These results can be explained by the low HMA stiffness and also by the low shear and pull-off resistance of the bond at 30 °C. With all this in mind, the consideration of the temperature-dependent HMA stiffness and interface bond properties appears to be reasonable for future use in pavement design.

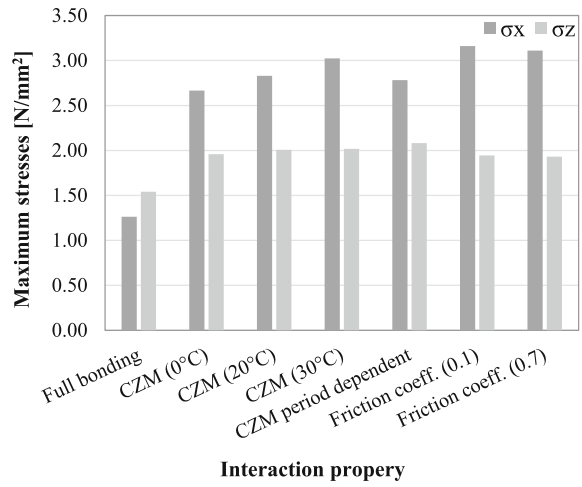
4.2 Design method

The developed FE-models for the computation of maximum stresses due traffic loads, which allow for the consideration of different interface modelling approaches, are part of a recently developed performance-based design procedure for bonded white topping overlays [26]. The design procedure is based on the Austrian design guide for the mechanistic-empirical design of new rigid pavements RVS 03.08.69 [16] and considers various structural parameters (i) the residual bearing capacity of the asphalt layer, (ii) the pavement structure including joint spacing, interface bonding conditions and the material properties, (iii) the traffic loading and (iv) the climatic conditions. It considers also the stresses due

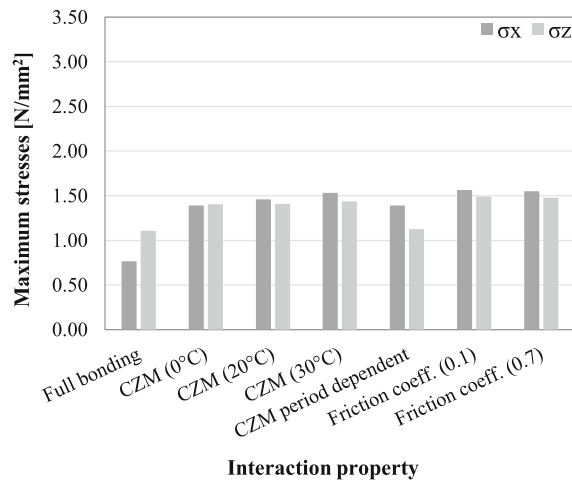




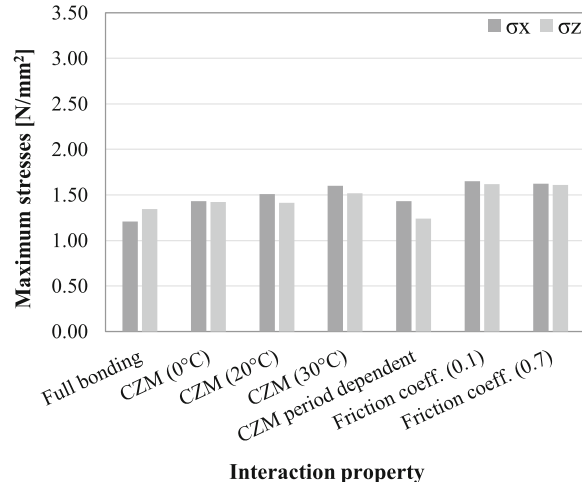
(a) Slab sizes 3 x 3 x 0.12 m



(b) Slab size 1.5 x 1.5 x 0.12 m



(c) Slab sizes 3 x 3 x 0.20 m



(d) Slab sizes 1.5 x 1.5 x 0.20 m

Fig. 7 Resulting maximum stresses due to traffic from different interface modelling approaches and slab geometries (seasonal period 4)

to temperature impact (curling stresses) with the revised Eisenmann’s model [48]. Representative temperature gradients were established for Austria in [49]. The service life (number of load cycles the pavement is able to resist) is calculated with the help of Smith’s fatigue criterion [50], which takes into account the maximum occurring curling and traffic stresses at the bottom of the concrete slab. In a next step, the partial damages for the different temperature periods are determined, which can be weighed and accumulated according to the superposition principle (Miner’s rule [51]) to estimate the design service life.

4.3 Design results and discussion

Using the above described design procedure and the resulting maximum stresses due to traffic from the different interface modelling approaches, the design service life expressed by the number of load cycles the pavement is able to resist N_{res} were estimated. The results from these estimations are given in Fig. 8. It is apparent that the interface bonding conditions play a crucial role in the resulting design life of slabs with a low thicknesses. Whereas, this effect is moderate for thicker slabs (slab thickness of 20 [cm]). Further, the

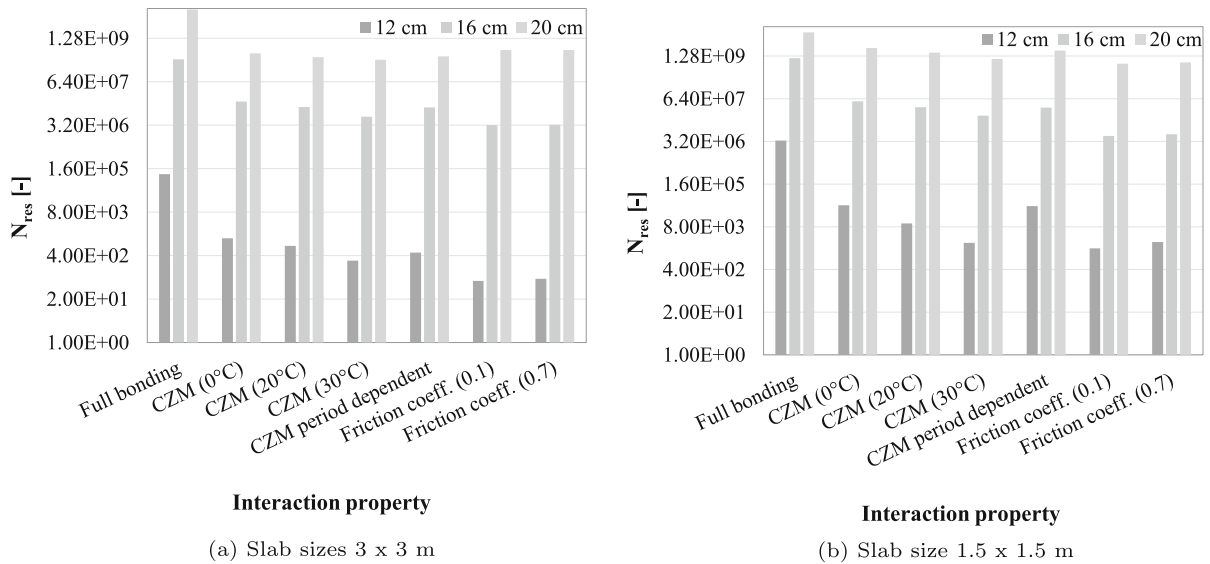


Fig. 8 Resulting design service lives from different interface modelling approaches and slab geometries

effect of different interface modelling approaches is more noticeable at pavements with smaller slab sizes.

The full bonding interface modelling approach yields the longest design life in all investigated cases. This corresponds to the lowest estimated stresses in Fig. 8. Considering the outcome of the stress analysis that this approach lacks of capability to account for the joints between the slabs, it shows the need to revise current design approaches.

The shortest design life is obtained from a simulation considering a friction coefficient of 0.1. An increase of the friction coefficient from 0.1 to 0.7 triggers an almost unnoticeable increase in the design life of thicker slabs (16 and 20 [cm]). This effect is more visible at a slab thickness of 12 [cm] with 14 % at slab size 3 x 3 [m] and 34 % at slab size 1.5 x 1.5 [m].

When comparing the resulting design life from the application of the CZM at different temperatures, it is noticeable that the consideration of temperature-dependent bond characteristics and stiffness of the HMA have a very big impact on the pavement performance. Corresponding to the stress analysis above, low HMA stiffness and CZM input parameters at 30 °C generate the shortest design life. The longest design life arises at CZM (0 °C). It should be noted here that the definition of cases, where a constant temperature is assumed over the year, is being performed only to demonstrate the impact of relevant input parameters and modelling approaches.

A more accurate way to consider those impact factors will be the derivation of input parameters to the CZM at different (and more than in this study) temperatures, estimation of the resulting stresses and their consideration through weighting in the final estimation of the design life. This approach was applied in the case named CZM period-dependent. On one hand, the application of a period-dependent interface bonding properties in the CZM results in a tremendous decrease of the design life in comparison to the full bonding approach. On the other hand, the resulting design life from the friction model with a friction coefficient of 0.7 is up to 90% lower compared to the CZM period dependent.

The most obvious finding to emerge from the analysis is that the implementation of empirical data to describe the interface bonding conditions in the normal and tangential direction leads to more realistic design results.

5 Conclusions

The impact of the interface bonding conditions on the occurring stresses due to traffic and on the design life of bonded concrete overlays of HMA was investigated. For that, different modelling approaches (full bonding model, friction model and CZM) were

utilised in different FE-models of pavement structures with various layer thicknesses and slab sizes.

Moreover, special attention has been given to the description of the CZM and the experimental derivation of temperature-dependent interface bonding data. This empirical data was implemented in the CZM and, therefore, creates the basis for a more realistic simulation of the interface bonding conditions. The application of the CZM as an appropriate interaction property between layers, was validated by a simulation of the static shear resistance test. It was demonstrated that the force-displacement curves from the test and from the simulation are in good agreement.

The following conclusions can be drawn from the experimental investigations of the interface behaviour in tangential and normal direction:

- The interface bond properties are strongly temperature dependent.
- The tensile strength decreases with the increase of the temperature and the conduction of tensile tests at high temperatures (30 °C and 40 °C) failed because of the low tensile strength of the HMA.
- The results from pull-off resistance tests and wedge-splitting tests are comparable.
- The shear strengths at low temperatures (−10 °C and 0 °C) are in the same range. A possible explanation for these results could be the fact that at low temperatures the adherent component of the bitumen is not activated and force transfer is ensured by temperature-independent aggregate interlocking.
- The early traffic release after concrete placement and the traffic load have a positive effect on the interface bond through the better compaction and generation of better aggregate interlocking.

The findings from the investigation of the effect of different modelling approaches on the relevant stresses and on the design life are summarized as follows:

- The effect of different interface modelling approaches on the relevant stresses due to traffic loads is more visible at slabs with lower thicknesses.
- Based on the stress analysis, it was found that the full bonding modelling approach induces the lowest stresses and can not adequately simulate the structural behaviour of the concrete overlay.

- The resulting design life is strongly depending on the applied interface modelling approach. This effect is more apparent at concrete overlays with low thicknesses and small slab sizes.
- The shortest design life results from the friction modelling approach. It is up to 90% lower than the resulting design life from the CZM with temperature-dependent interface data.
- The relevance of implementing temperature-dependent empirical data to describe the interface bonding conditions in the pavement structural models is clearly supported by the current findings.

Acknowledgements The authors gratefully acknowledge financial support from the Austrian Research Promotion Agency (FFG) through project “EcoRoads sustainable rigid pavements” and the Research Association “Sustainable rigid pavements”. Furthermore, the authors would like to express their gratitude to TU Wien Bibliothek for the financial support through its Open Access Funding Programme.

Funding Open access funding provided by TU Wien (TUW).

Declarations

Conflicts of interest The authors declare that there are no conflicts of interest in this research.

Open Access This article is licensed under a Creative Commons Attribution 4.0 International License, which permits use, sharing, adaptation, distribution and reproduction in any medium or format, as long as you give appropriate credit to the original author(s) and the source, provide a link to the Creative Commons licence, and indicate if changes were made. The images or other third party material in this article are included in the article’s Creative Commons licence, unless indicated otherwise in a credit line to the material. If material is not included in the article’s Creative Commons licence and your intended use is not permitted by statutory regulation or exceeds the permitted use, you will need to obtain permission directly from the copyright holder. To view a copy of this licence, visit <http://creativecommons.org/licenses/by/4.0/>.

References

1. Delatte NJ, Fowler DW, McCullough BF, Grater SF (1998) Investigating performance of bonded concrete overlays. *J Perform Cons Facil* 12(2):62–70. [https://doi.org/10.1061/\(ASCE\)0887-3828\(1998\)12:2\(62\)](https://doi.org/10.1061/(ASCE)0887-3828(1998)12:2(62))
2. Tschegg EK, Kroyer G, Tan DM, Stanzl-Tschegg SE, Litzka J (1995) Investigation of bonding between asphalt layers on road constructions. *J Transp Eng Asce* 121:309–316
3. Canestrari F, Ferrotti G, Partl MN, Santagata E (2005) Advanced testing and characterization of interlayer shear



- resistance. *Transp Res Record* 1929(1):69–78. <https://doi.org/10.1177/0361198105192900109>
4. Raab C, Partl MN (2009) Interlayer bonding of binder, base and subbase layers of asphalt pavements: long-term performance. *Cons Build Mater* 23:2926–2931. <https://doi.org/10.1016/j.conbuildmat.2009.02.025>
 5. Raab C, Grenfell J, Abd El Halim AO, Manfred Norbert Partl MN (2015) The influence of age on interlayer shear properties. *Int J Pavement Eng* 16(6):559–569. <https://doi.org/10.1080/10298436.2014.943212>
 6. Cho S, Kim YR (2016) Verification of time-temperature superposition principle for shear bond failure of interlayers in asphalt pavements. *Transp Res Record* 2590(1):18–27. <https://doi.org/10.3141/2590-03>
 7. Ragni D, Sudarsanan N, Canestrari F, Kim YR (2021) Investigation into fatigue life of interface bond between asphalt concrete layers. *Int J Pavement Eng* 23(10):1–15. <https://doi.org/10.1080/10298436.2021.1894420>
 8. Leng Y, Al-Qadi IL, Samuel SHH, Carpenter Ozer H (2009) Interface bonding between hot-mix asphalt and various portland cement concrete surfaces: Assessment of accelerated pavement testing and measurement of interface strain. *Transp Res Record* 2127(1):20–28. <https://doi.org/10.3141/2127-03>
 9. Ozer H, Al-Qadi I, Wang H, Leng Z (2012) Characterisation of interface bonding between hot-mix asphalt overlay and concrete pavements: modelling and in-situ response to accelerated loading. *Int J Pavement Eng* 13(2):181–196. <https://doi.org/10.1080/10298436.2011.596935>
 10. Zhao H, Cao J, Zheng Y (2017) Investigation of the interface bonding between concrete slab and asphalt overlay. *Road Mater Pavement Design* 18(sup3):109–118. <https://doi.org/10.1080/14680629.2017.1329866>
 11. Bayraktarova K, Dimitrov M, Hofko B, Eberhardsteiner L (2020) Behaviour of the interface bonding between asphalt overlays and rigid pavements In: *In Proceedings of the 9th International Conference on Maintenance and Rehabilitation of Pavements*. Springer, Cham
 12. Hart J (2000) Evaluation of bonding between ultra-thin portland cement concrete overlays and asphalt cement concrete. Master's thesis, Iowa State University, Ames
 13. Mateos A, Harvey J, Paniagua J, Paniagua F, Fan A (2016) Role of concrete-asphalt interface in bonded concrete overlays of asphalt pavements. In: Chabot A, Buttlar WG, Dave EV, Petit C, Tebaldi G (eds) 8th RILEM international conference on mechanisms of cracking and debonding in pavements. Springer, Dordrecht, pp 489–494
 14. ARA I (1993) AASHTO guide for design of pavement structures. ERES Division of ARA, Inc., 505 West University Avenue Champaign, Illinois 61820
 15. ARA I (2004) Guide for mechanistic-empirical design of new and rehabilitated pavement structures. National Academy of Science., Washington, DC
 16. FSV: (2020) RVS 03.08.69: Rechnerische Dimensionierung von Betonstraßen. Österreichische Forschungsgesellschaft Straße-Schiene-Verkehr, Vienna
 17. FGSV: (2012) Richtlinien Für die Standardisierung des Oberbaus von Verkehrsflächen (RStO). Forschungsgesellschaft für Straßen- und Verkehrswesen, Cologne, Germany
 18. FGSV: (2013) Merkblatt Für die Whitetopping–Bauweise (M WT). Forschungsgesellschaft für Straßen- und Verkehrswesen, Köln, Germany
 19. Vandenbosche J, Dufalla N, Li Z (2017) Bonded concrete overlay of asphalt mechanicalempirical design procedure. *Int J Pavement Eng* 18(11):1004–1015. <https://doi.org/10.1080/10298436.2016.1141410>
 20. Harrington D, Fick G (2014) Guide to concrete overlays: sustainable solutions for resurfacing and rehabilitating existing pavements (3rd Edn). National Concrete Pavement Technology Center, Ames
 21. Torres HN, Roesler J, Rasmussen RO, Harrington D (2014) Guide to the design of concrete overlays using existing methodologies. Technical report, Institute of Transportation, Iowa State University, Ames
 22. Chavez MCI, Choi SC, Won M (2007) Concrete pavement overlays and failure mechanisms. Technical report, Center for Transportation Research, The University of Texas at Austin, Austin
 23. ACPA (2013) Concrete Overlay on Asphalt (BCOA) Thickness designer [online]. American Concrete Pavements Association, Rosemont
 24. Eberhardsteiner L, Bayraktarova K, Wagner E, Peyerl M, Gschösser F, Blab R (2020) Sustainable concrete roads—project report for the second year of research. Technical report, Vienna University of Technology, Institute of Transportation, Vienna
 25. Eberhardsteiner L, Bayraktarova K, Peyer MJ, Longi P, Peyerl M, Gschösser F, Blab R (2021) Sustainable concrete roads—project report for the third year of research. Technical report, Vienna University of Technology, Institute of Transportation, Vienna
 26. Bayraktarova K, Eberhardsteiner L, Peyer JM, Blab R (2023) Performance based design of bonded whitetopping overlays. *Road Mater Pavements Design* 1–15. <https://doi.org/10.1080/14680629.2022.2164331>
 27. Bek J, Al-Qadi IL (2006) Finite element method modeling of reflective cracking initiation and propagation: investigation of the effect of steel reinforcement interlayer on retarding reflective cracking in hot-mix asphalt overlay. *Transp Res Record J Transp Res Board* 1949:32–42. <https://doi.org/10.1177/03611981061949001>
 28. Song SH, Paulino GH, Buttlar WG (2006) A bilinear cohesive zone model tailored for fracture of asphalt concrete considering viscoelastic bulk material. *Eng Fract Mech* 73(18):2829–2848. <https://doi.org/10.1016/j.engfracmech.2006.04.030>
 29. Olubanwo A, Karadelis NJ (2015) Interfacial delamination failure in bonded concrete overlay systems / a review of theories and modelling methods. *Int J Civ Eng Technol* 6(5):85–99
 30. Bari ME, Zollinger DG (2016) New concepts for the assessment of concrete slab interfacial effects in pavement design and analysis. *Int J Pavement Eng* 17(3):233–244. <https://doi.org/10.1080/10298436.2014.993183>
 31. Dave EV, Behnia B (2018) Cohesive zone fracture modelling of asphalt pavements with applications to design of high-performance asphalt overlays. *Int J Pavement Eng* 19(3):319–337. <https://doi.org/10.1080/10298436.2017.1353393>



32. Barenblatt G (1959) The formation of equilibrium cracks. During brittle fracture. General ideas and hypotheses axially-symmetric cracks. *J Appl Math Mech* 23(3):622–636. [https://doi.org/10.1016/0021-8928\(59\)90157-1](https://doi.org/10.1016/0021-8928(59)90157-1)
33. Dugdale DS (1960) Yielding of steel sheets containing slits. *J Mech Phys Solids* 8(2):100–104. [https://doi.org/10.1016/0022-5096\(60\)90013-2](https://doi.org/10.1016/0022-5096(60)90013-2)
34. Xu X-P, Needleman A (1994) Numerical simulations of fast crack growth in brittle solids. *J Mech Phys Solids* 42(9):1397–1434. [https://doi.org/10.1016/0022-5096\(94\)90003-5](https://doi.org/10.1016/0022-5096(94)90003-5)
35. Camacho GT, Ortiz M (1996) Computational modelling of impact damage in brittle materials. *Int J Solids Struct* 33(20):2899–2938. [https://doi.org/10.1016/0020-7683\(95\)00255-3](https://doi.org/10.1016/0020-7683(95)00255-3)
36. Geubelle PH, Baylor JS (1998) Impact-induced delamination of composites: a 2D simulation. *Compos Part B Eng* 29(5):589–602. [https://doi.org/10.1016/S1359-8368\(98\)00013-4](https://doi.org/10.1016/S1359-8368(98)00013-4)
37. Espinosa HD, Zavattieri PD (2003) A grain level model for the study of failure initiation and evolution in polycrystalline brittle materials. Part i: theory and numerical implementation. *Mech Mater* 35(3–6):333–364. [https://doi.org/10.1016/S0167-6636\(02\)00285-5](https://doi.org/10.1016/S0167-6636(02)00285-5)
38. Soares JB, de Freitas F, Allen D (2003) Considering material heterogeneity in crack modeling of asphaltic mixtures. *Transp Res Record J Transp Res Board* 1832:113–120. <https://doi.org/10.3141/1832-1>
39. Paulino GH, Zhang ZY (2004) Cohesive zone modeling of fracture in asphalt concrete. In: *Proceedings of the 5th International RILEM Conference—cracking in Pavements: Mitigation, Risk Assessment, and Preservation*, Limoges, France, pp. 63–70
40. Olubanwo A (2014) Optimum design for sustainable green bonded concrete overlays: failure due to shear and delamination. PhD thesis, Coventry University, Coventry
41. Smith M (2014) ABAQUS/Standard user's manual, Version 6.14. Dassault systèmes Simulia Corp, United States
42. ÖNI: (1997) ÖNORM B 3639-2: Technische Asphalte für den Aßenbau und Verwandte Gebiete - Prüfung - Haftverbund von Asphaltschichten. Österreichisches Normungsinstitut, Vienna
43. FSV: (2016) RVS 13.01.51: Betonstraßen - Betondeckenerhaltung. Österreichische Forschungsgesellschaft Straße-Schiene-Verkehr, Vienna
44. ÖNI: (1997) ÖNORM B 3639-1: Technische Asphalte für den Straßenbau und verwandte Gebiete - Prüfung—Schubverbund von Asphaltschichten. Österreichisches Normungsinstitut, Vienna
45. ÖNI: (2011) ÖNORM B 3592 - Bestimmung der Kerbspaltzugfestigkeit und der spezifischen Bruchenergie von Baustoffen, Baustoffverbindungen und Verbundwerkstoffen. Österreichisches Normungsinstitut, Vienna
46. Salve AK, Sudhindra SN (2015) Implementation of cohesive zone in abaqus to investigate fracture problems. In: *National conference for engineering post graduates RIT NConPG-15*, pp 60–66
47. Peyerl M, Krispel S, Weihs P, Maier G (2016) Stadtverkehrsflächen—optimierter Beton für den innerstädtischen Bereich. *Aktuelles zu Betonstrassen und zur Verkehrsinfrastruktur*, 44(1)
48. Houben ILJM (2009) Structural design of pavements. TU Delft . <http://www.citg.tudelft.nl/en/about-faculty/departments/structural-engineering/sections/pavement-engineering/education/lectures/>
49. Bayraktarova K, Eberhardsteiner L, Zhou D, Blab R (2021) Characterisation of the climatic temperature variations in the design of rigid pavements. *Int J Pavement Eng* 23(9):3222–3235. <https://doi.org/10.1080/10298436.2021.1887486>
50. Eisenmann J, Leykauf G (2003) Concrete pavements—design and construction (in German). Ernst and Sohn, Munich
51. Miner MA (1945) Cumulative damage in fatigue. *J Appl Mech* 12(3):159–164. <https://doi.org/10.1115/1.4009458>

Publisher's Note Springer Nature remains neutral with regard to jurisdictional claims in published maps and institutional affiliations.

